Available online at www.sciencedirect.com
ScienceDirect
Geochimica et Cosmochimica Acta 71 (2007) 2975–2988
Geochimica et Cosmochimica Acta
www.elsevier.com/locate/gca

Analysis of the climate signal contained within $\delta^{18}O$ and growth rate parameters in two Ethiopian stalagmites

Andy Baker [a,*], Asfawossen Asrat [b], Ian J. Fairchild [a], Melanie J. Leng [c,d], Peter M. Wynn [a], Charlotte Bryant [e], Dominique Genty [f], Mohammed Umer [b]

[a] School of Geography, Earth & Environmental Sciences, The University of Birmingham, Birmingham B15 2TT, UK
[b] Department of Earth Sciences, Addis Ababa University, P.O. Box 1176, Addis Ababa, Ethiopia
[c] NERC Isotope Geosciences Laboratory, British Geological Survey, Keyworth, Nottingham NG12 5GG, UK
[d] School of Geography, University of Nottingham, Nottingham NG7 2RD, UK
[e] NERC Radiocarbon Laboratory, Scottish Enterprise Technology Park, Rankine Avenue, East Kilbride G75 OQF, UK
[f] Laboratoire des Sciences du Climat et de l'Environnement (LSCE), CNRS/CEA, L'Orme des Merisiers, 91400 Gif-sur-Yvette, France

Received 13 October 2006; accepted in revised form 23 March 2007; available online 13 April 2007

Abstract

We combine surface and cave climate monitoring with multiple stalagmite parameters to help understand and calibrate the climate records contained within stalagmites from a region with strong rainfall seasonality. Two actively growing stalagmites from Ethiopia were analysed in order to investigate the climate signal contained within $\delta^{18}O$ and growth rate parameters. The $\delta^{18}O$ and growth rate of the two stalagmites give different responses to surface climate due to variations in the climate signal transfer. Both stalagmites (Merc-1 and Asfa-3) have a climate response that is seasonal; however this signal is subsequently smoothed by the mixing of event and storage water within the aquifer. Merc-1 responds more to high frequency ('event') climate, due to a greater ratio of event to storage water in this sample, whereas Asfa-3 responds more to low frequency ('storage') climate. In addition, different parameters respond to different seasons. For example, stalagmite Asfa-3, from greater depth from the surface and with a slow drip rate, has a growth rate that responds to the amount of summer rain. In contrast, Merc-1, closer to the surface and with a faster drip rate, exhibits no clear response to surface climate, probably due to a more complex climate signal transfer. $\delta^{18}O$ response varies with stalagmite due to the interplay between rainfall forcing factors (amount, seasonality) and disequilibrium kinetics, with opposing correlations between seasonal rainfall and $\delta^{18}O$ between the samples. Our results demonstrate that analysis of seasonal climate forcing, and transfer functions reflecting the mixing of event and storage water, may be the most appropriate approach to develop of transfer functions appropriate for high-resolution, stalagmite climate reconstruction.

1. INTRODUCTION

The African climate system, and its surrounding monsoons, is a key element of the global atmospheric circulation. Rainfall is, in many parts of Africa, dependent on prevailing patterns of sea surface temperature (SST), atmospheric winds, the El Niño Southern Oscillation (ENSO), and regional climate fluctuations in the Indian and Atlantic Oceans. Much remains to be understood about the interaction between the African climate system and its land surface, and the surrounding ocean-atmosphere climate variability and the global climate system. The Ethiopian highlands are a classic example of such an African rain-sensitive region, where future forecasts are hampered by inadequate understanding of historical patterns, their wider associations, and causes. Rainfall and temperature records are relatively short and of poor quality (see overview by Conway et al., 2004). The few long records demonstrate

* Corresponding author. Fax: +44 121 4155824.
E-mail address: a.baker.2@bham.ac.uk (A. Baker).

0016-7037/$ - see front matter © 2007 Elsevier Ltd. All rights reserved.
doi:10.1016/j.gca.2007.03.029

that after El Niño years, the spring rains are heavy and the main summer rains are reduced (Glantz, 1996). This agrees with a strong multi-year spectral peak in rainfall records for the region that correlates with Atlantic and Indian Ocean SSTs (Nicholson, 2000). However, the calibration period is short and this correlation is too weak to enable drought forecasts. In addition, the spring rains also fail and lead to famine; their cause is more complicated with a dependence on a low-level moisture influx towards Ethiopia and an upper trough with cooling in the mid-upper troposphere (Camberlin and Philippon, 2002). Spring rainfall failures are, to date, not predictable. Long, high-resolution climate records are required to investigate the nature of rainfall variability, the frequency of failure of either rain period, as well as to investigate the presence of longer term periodicity in climate that cannot be detected through short instrumental series. A particularly powerful approach is to make use of well-dated proxy material to derive independent tests of past climate variability. Lake records have been widely studied, and include lake level records (Gillespie et al., 1983), and core studies of diatom, stable isotope and pollen proxies (see reviews by Lamb, 2001; Mohammed et al., 2004). However, despite the presence of proven biochemical varves in some lakes (Lamb et al., 2002), high-resolution climate reconstructions are so far hampered by poor chronological constraints. Recent rapid advances in the understanding of the climatic meaning of parameters derived from calcareous speleothems (cave precipitates), indicates that speleothem records are the best prospect for tackling this urgent problem in East Africa.

Speleothems are known to provide high-resolution climate records (e.g., Tan et al., 2006) and the study of calcareous speleothems as archives of climate change is a major area of paleoclimate research (e.g., reviews in McDermott et al., 2005; Fairchild et al., 2006a). A multi-proxy approach in stalagmite palaeoclimate reconstruction is crucial because the various proxies respond differently (rapidly, lagged, linearly, non-linearly) or with different degrees of smoothing to climate signals (Asrat et al., 2007; Fairchild et al., 2006a), depending on the processes affecting speleothem deposition. These are rapidly becoming more completely understood (McDermott et al., 2005; Fairchild et al., 2006a). Firstly, in favourable circumstances, primary atmospheric signals, such as the oxygen isotopic composition of rainfall, can be directly reflected in the variation of $\delta^{18}O$ values of speleothem $CaCO_3$ with time. This is the primary mode of variation of $\delta^{18}O$ in monsoonal climates in central-southern and eastern China, and Oman, where there is a strong "amount" effect on rainfall (Neff et al., 2001; Burns et al., 2002; Fleitmann et al., 2003; Wang et al., 2005). Secondly, the vegetation and soil overlying the cave can modify atmospheric signals to a varying extent (e.g. preferential recharge of intense rains) and generate new signals (e.g. $\delta^{13}C$ and trace elements). Thirdly, the karst system leads to variable mixing of infiltrating waters and the processes of degassing and carbonate precipitation modify fluid chemistry leading to heavier $\delta^{13}C$ values. Where evaporation occurs, there are shifts to heavier $\delta^{18}O$, and both degassing and evaporation are characteristically better expressed during climatically dry intervals (Raisback et al., 1994). In a monsoonal climate, the effect on $\delta^{18}O$ on within-cave processes, would be to reinforce shifts related to changes in the quantity of rainfall. However, in high-resolution records, it becomes necessary to separate these different effects in order to derive quantitative records and this can be done by locating characteristic co-variations that can be attributed to evaporation (e.g. $\delta^{13}C$ versus $\delta^{18}O$). In addition, there are other independent parameters that can be calibrated with the instrumental record. For example, stalagmite growth rates can be characteristic functions of drip water chemistry and drip rate (Baker et al., 1998; Dreybrodt, 1988; Genty et al., 2001) and there are also theoretical expectations for changing lamina and stalagmite shape in response to drip rate (Kaufmann and Dreybrodt, 2004).

Because each speleothem is fed by a unique plumbing system, there is always the possibility of contingent variation related to factors unique to that drip (i.e. plumbing reorganization), and in principle each speleothem may have different sensitivities and thresholds to change (Smart and Friedrich, 1987; Baker and Brunsdon, 2003; Fairchild et al., 2006b). For this reason, there is a need to at least duplicate samples wherever possible, and to establish records involving multiple parameters to check for internal consistency, and to account for unique hydrological factors for a given drip from changes affecting whole caves or different caves in a region. Comparison with modern instrumental records is particularly useful in establishing the nature of modern transfer functions which exist between speleothem and climatic parameters, and to establish the responses (e.g. rapid, lagged, linear, non-linear), or degree of smoothing. These are the foci of this paper. We report the results of our recent expeditions to the Ethiopian karst, where we have collected stalagmites to undertake a multi-proxy climate reconstruction. This has included the collection of drip and pool water samples for isotopic and geochemical analysis, the measurement of cave temperature and humidity, the analysis of regional climate data and the collection of actively growing stalagmite samples. These results provide a modern baseline from which we can understand contemporary processes and calibrate stalagmite parameters against instrumental climate records before one can then reconstruct past climate, and in particular precipitation, variability from stalagmites in Ethiopia.

2. SITE DESCRIPTION

2.1. Climate

Contrasting climate processes determine the spatial and temporal patterns of rainfall in Ethiopia (Fig. 1). The main rainy season (July–September) occurs when the northward movement of the Inter-Tropical Convergence Zone (ITCZ) dominates the airflow. This in itself produces rain, but rainfall is also generated by the development and persistence of Arabian and Sudan thermal lows at 20°N latitude, the development of the tropical easterly jet and its persistence, and the generation of the low-level 'Somali jet' that enhances low-level southwesterly flow (Seleshi and Zanke, 2004). The spring rainy season (March–May) coincides

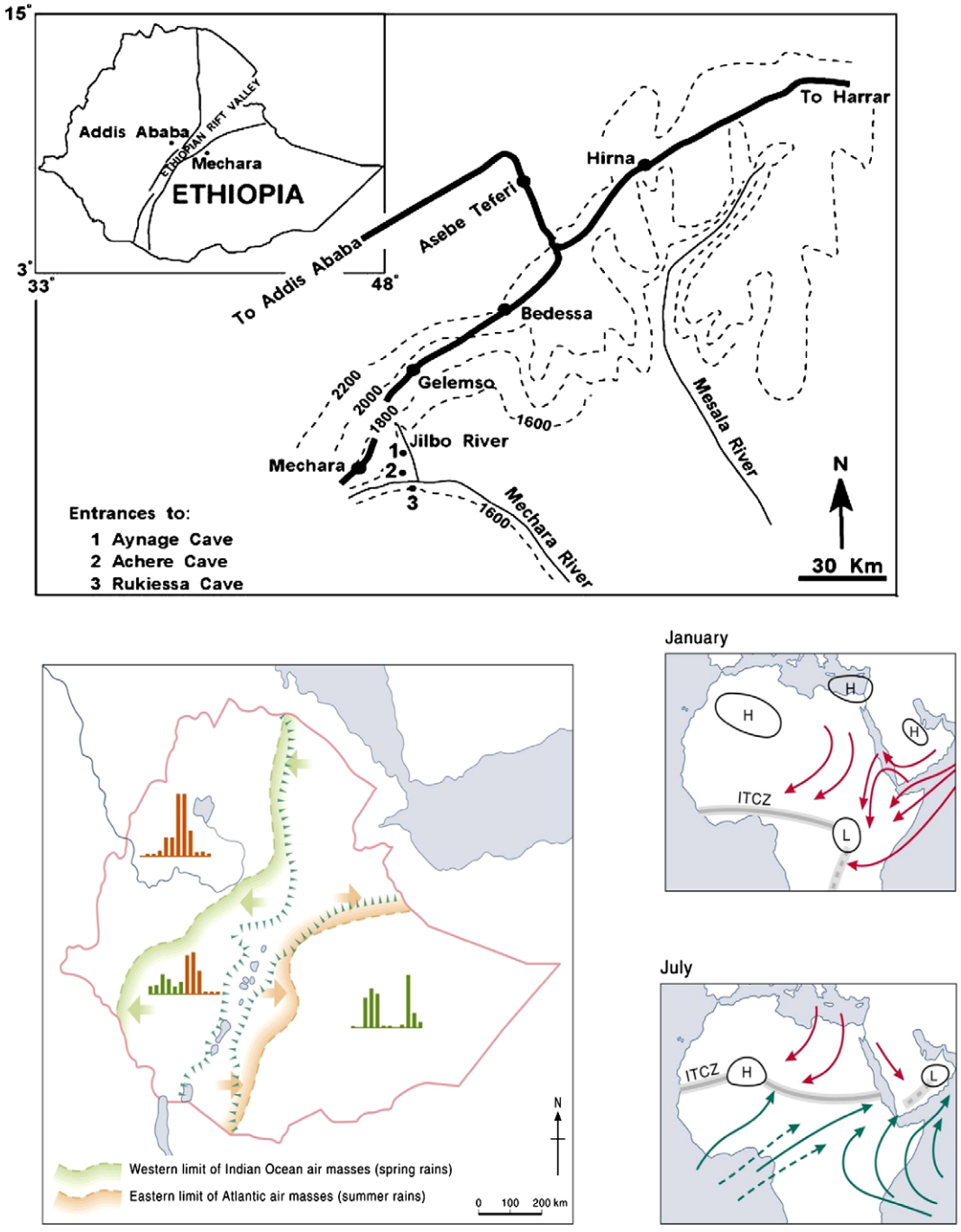

Fig. 1. (top) Location of sample site; weather stations are located at Mechara, Gelemso, and Bedessa. (base) Schematic of Ethiopian climate; histograms show monthly rainfall totals.

with the southward migration of the ITCZ and the associated movement of the Arabian high towards the north Arabian Sea, allowing the development of a thermal low over the south of Sudan, with moist easterly winds drawn towards this low producing the spring rains in Ethiopia. These contrasting processes generate distinct isotopic composition of the rainfall. Modern precipitation $\delta^{18}O$ (monthly data from Addis Ababa since 1970) demonstrate a maximum annual range of $\delta^{18}O$ of 14‰ (−6.1‰ to +7.9‰). The summer rains (e.g. July $\delta^{18}O = -1.8 \pm 1.8$‰; range −4.4‰ to +1.3‰) are isotopically lighter than spring (e.g. April $\delta^{18}O = +1.5 \pm 1.8$‰; range −1.9‰ to +6.1‰) rainfall $\delta^{18}O$. From the limited IAEA dataset there appears to be a much more significant relationship with the source of rainfall than temperature or amount effects within each period (Leng et al., 1998).

Variability in the movement of the ITCZ causes most of the interannual variability in rainfall over Ethiopia (Seleshi and Zanke, 2004), with the dynamics of the ITCZ known to be teleconnected to El Niño (Nicholson, 2000), most likely

via changes in Indian Ocean sea surface temperature. Comparison of these processes with long rainfall records, however, is hampered by a lack of good quality records in the region. For example, in a recent analysis of 43 stations with more than 15 years of data, only 11 stations had rainfall data with <10% missing values in any given year (Seleshi and Zanke, 2004). Analysis of the longest existing rainfall record in the country at Addis Ababa (Addis Ababa Observatory; 1898–2002 record), however, showed that these data can be used with a good level of certainty for further comparison (Conway et al., 2004).

2.2. Caves

Caves in the Mechara karst were first discovered by the Huddersfield Expedition in 1996 (Brown et al., 1998), for location see Fig. 1. The Mechara karst area is located in Southeastern Ethiopian plateau and lies at the foot of a long mountain ridge formed by Oligocene flood basalts. The ridge marks the southeastern margin of the NE–SW trending Ethiopian rift valley. The Mechara karst system developed on Jurassic limestone beds (the Antalo Limestone Unit; Bosellini et al., 1997; Asrat, 2002). The Antalo Limestone unit with a total estimated thickness of 400 m consists of thin, fossiliferous limestone beds intercalated with marl and sandy limestone beds at the top, and massive, crystalline limestone beds intercalated with thin marl and mudstone beds at the bottom. The Antalo Limestone unit is conformably overlain by Jurassic shale (Agula Shale unit) with an estimated thickness of 150 m which comprises variegated shale, marl, and mudstone intercalated with thin beds of crystalline limestone and rarely dolomite. A Cretaceous sandstone (Ambaradam Formation) conformably overlies the Agula shale. The Ambaradam Formation with a total thickness of 100 m, consists of white to pink, medium to coarse-grained, immature, clastic sandstone beds intercalated with silt, shale, mudstone, laterite beds, and quartz conglomerates.

Most of the caves are easily accessible, have been surveyed in detail, require no technical caving skills to explore, and, most importantly, contain actively growing and dripping stalagmites suitable for monitoring and climate analysis. One such cave is Rukiessa Cave, currently surveyed to approximately 1.3 km length and a total depth of 192 m from the surface; the survey is currently unpublished and so a short cave description is provided here. The Rukiessa Cave is a tight, vertical passageway formed along vertical fractures truncated by horizontal ''chambers'' formed following bedding planes. The cave is wet and regularly flashed by seasonal floods. The cave is accessed through a vertical hole in the ground. The entrance chamber is a spacious room of about 15 m height and nearly 6 m by 6 m area. A very tight, vertical passageway drops down and gives way to the entrance of the Mercury chamber lying lies right beneath the entrance chamber, at an approximate depth of 25 m below the surface. This chamber is a very narrow opening of 1 m height and 3 m by 3 m area. The roof of this chamber is decorated by active stalactites which feed some active stalagmites including Merc-1 stalagmite. The Mercury chamber at its eastern end gives way to another spacious chamber which is filled by big limestone blocks fallen from the roof and walls. Asfa Chamber is a tight 2 m by 4 m opening beneath this spacious chamber, at an approximate depth of 30 m from the surface. This chamber is very wet, where pool waters are fed by drips from active stalactites at the roof, and flowing cave streams are common. Several active and non-corroded stalagmites, including Asfa-3, are present in this chamber. At its western end, this chamber gives way to an abrupt vertical drop which forms a 20 m deep hollow pit beneath.

The Rukiessa Cave is overlain by ploughed fields where maize, millet, coffee and chat are the major vegetation types planted. The scattered trees and scrub remnants between fields attest that the area has been affected by clearance and agricultural impacts. Residual soils of <1 m thickness have developed over the sandy limestone that constitutes the roof of the cave.

3. METHODS

3.1. Surface and cave climate

Three weather stations operated by the Ethiopian Meteorological Service Agency (NMSA) exist within the study region. These are sited at Mechara, Gelemso and Bedessa (see Fig. 1 for their location). They are all of grade 3 of the NMSA, which is the lowest grade, highlighting data that is discontinuous and potentially inhomogenous. Data availability was 1968–1976; 1998- (Mechara, 1790 m a.s.l., 40°19′E, 08°36′N), 1969–1991; 2001- (Gelemso, 1800 m a.s.l.) and 1967–1974; 1980–1991; 1994- (Bedessa, 1820 m a.s.l., 40°46′E, 08°55′N) for monthly mean rainfall and 1973–1974; 1986–1991 (Gelemso) and 1968–1974; 1981–1991; 1994 (Bedessa) for monthly mean maximum and minimum temperature. As far as possible with such short data series, rainfall, and temperature data were tested for homogeneity, and compared to the nearest long homogenous climate series, that at Addis Ababa (400 km to the Northwest) to generate a corrected rainfall series for the region based on the Addis Ababa returns.

Cave climate data was obtained through the use of Kestrel handheld weather stations and Tinytag temperature loggers during visits to Rukiessa Cave in April 2004, January 2005 and October 2005. Handheld stations were used to record temperature and relative humidity at different locations within the cave: results are accurate to ±1 °C and ±3% relative humidity, with an upper measurement limit of 95%. Tinytag temperature loggers were left in the cave to record temperature variation through time from October 2005: loggers have a quoted accuracy of 0.25 °C.

3.2. Surface and ground water geochemistry

Various surface and ground waters were sampled from the region during sampling trips in April 2004, January 2005 and October 2005. Surface water samples include surface rivers and springs, while cave samples include stagnant pools, flowing cave streams and drip waters. Water samples were collected in 60 or 30 ml HDPE bottles. On return from the field, samples were analysed for pH and electrical con-

ductivity using a WTW 340i Multimeter. Samples for isotope analysis were then immediately transferred to fill an 8 ml HDPE bottle. For isotopic analysis, the waters were equilibrated with CO_2 using an Isoprep 18 device for oxygen isotope analysis with mass spectrometry performed on a VG SIRA. For hydrogen isotope analysis, an on-line Cr reduction method was used with a EuroPyrOH-3110 system coupled to a Micromass Isoprime mass spectrometer. Isotopic ratios ($^{18}O/^{16}O$ and $^{2}H/^{1}H$) are expressed in delta units, $\delta^{18}O$ and $\delta^{2}H$ (‰, parts per mille), and defined in relation to the international standard, VSMOW (Vienna Standard Mean Ocean Water). Analytical precision is typically ±0.05‰ for $\delta^{18}O$ and ±1.0‰ for $\delta^{2}H$. In October 2005, a sub-sample was filtered in the field (Whatman GF/C) and acidified with a drop of concentrate HNO_3 for cation analyses, which were performed by ICP-AES at the NERC facility, Royal Holloway, University of London.

3.3. Stalagmites

Two stalagmite samples, that were being actively dripped upon when collected, have been used in this study. They both had drip water electrical conductivity of >700 μS cm^{-1} indicative of calcite supersaturation. Asfa-3 was sampled from Asfa Chamber, Merc-1 from Mercury Chamber (Fig. 2). Both were between 50 and 100 mm high, and when sectioned had continuous visible laminae. One half of each stalagmite was polished for morphological analysis and lamina counting using image analysis. The unpolished half was used for geochemical analyses. For each stalagmite, the following methods were used:

(1) Analysis of stalagmite morphology (after Gams, 1981; Dreybrodt and Franke, 1987; Kaufmann and Dreybrodt, 2004) and calcite texture and fabric (after Kendall and Broughton, 1978; Genty and Quinif, 1996; Frisia et al., 2000, 2002). Stalagmite shape has been a neglected area of stalagmite analysis, but provides a direct indication of variations in drip hydrology. Stalagmite texture and fabric can be related to drip hydrology, drip water supersaturation, and cave climatic conditions, and potentially provides an indication of possible disequilibrium isotope composition. Texture variations have been observed to be commonplace in Ethiopian stalagmites (Asrat et al., 2007).

(2) Measurement of growth rate derived from visible lamina widths (Genty and Quinif, 1996; Genty et al., 1997, 2001). Growth rate has a well understood relationship with surface climate, primarily driven by the production of soil CO_2 due to changes in temperature and moisture (Dreybrodt, 1981; Baker et al., 1998). Lamina counting was conducted on a scanned high-resolution image of the polished stalagmite using image processing software (Image Pro Plus 5.0) using the protocols outlined in Tan et al. (2006). The image was enhanced, by stretching the observed range of pixel intensities to the maximum possible (full 0–255 range), and lamina widths calculated by measuring the average distance between visible laminae using a ~50 pixel wide transect. Triplicated lamina profiles were counted.

(3) Oxygen and carbon isotopes provide a record of one or all of rainfall source variations, temperature, or kinetic fractionation (McDermott et al., 2005). Samples for stable isotope measurements were drilled at regular intervals along the central growth axis of the speleothems (labelled O on Fig. 2). To avoid aliasing effects, we drilled time integrated samples of 3–5 years (1–3 mm depending on growth rate) duration. In addition, samples were drilled laterally along growth laminae, in order to investigate the lateral changes in isotope composition (the 'Hendy test', labelled H on Fig. 2). Analyses were conducted at the NERC Isotope Geosciences Laboratory at Keyworth. The calcite samples were reacted with phosphoric acid and cryogenically purified before mass spectrometry using an Isocarb plus Optima dual-inlet mass spectrometer. By comparison with a laboratory marble standard, the sample $^{18}O/^{16}O$ and $^{13}C/^{12}C$ ratios are reported as $\delta^{18}O$ and $\delta^{13}C$ values in per mille (‰) versus VPBD. Analytical precisions are <0.1‰ for the standard marble.

(4) The ^{14}C activity of modern speleothems is used to confirm the active deposition of our two samples. Stalagmites record the atmospheric ^{14}C bomb input superimposed on the ^{14}C signal from 'dead carbon' that has derived from

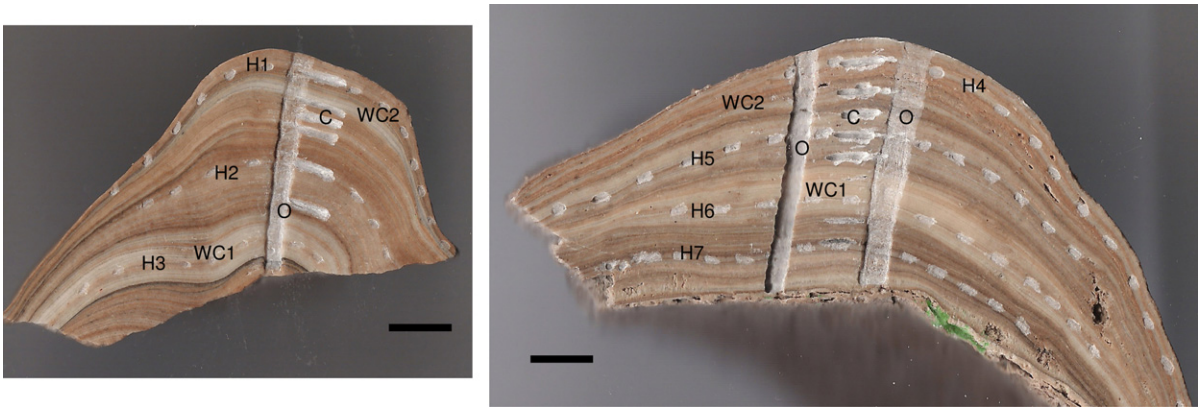

Fig. 2. Stalagmites Asfa-3 (left) and Merc-1 (right). $\delta^{18}O$ profiles are vertical suites of samples labelled 'O' (duplicate analyses on Merc-1). Samples for Hendy tests are horizontal drill samples along laminae (labelled 'H1-7'; three on Asfa-3, four on Merc-1). Five ^{14}C analyses (label 'C') are also visible on each sample (the sixth analysis is on the stalagmite top). 1 cm scale bars shown.

limestone dissolution (Genty and Massault, 1997, 1999; Genty et al., 1998, 2001). Stalagmite 'dead carbon proportion' is typically $15 \pm 10\%$, and the superimposed 'bomb carbon' signal is both damped and has a time delay between 1964 (date of the atmospheric ^{14}C peak) and the maximum of ^{14}C activity observed in the stalagmite, due primarily to soil carbon cycling. Speleothem samples were drilled (labelled C on Fig. 2) and stored under argon until hydrolysis to CO_2 using 85% H_3PO_4 at 25 °C. Carbon dioxide was cryogenically separated. Aliquots of CO_2 were converted to an iron/graphite mix by iron/zinc reduction (Slota et al., 1987). A sub-sample of CO_2 was used to measure $\delta^{13}C$ using a dual-inlet mass spectrometer with a multiple ion beam collection facility (VG OPTIMA) in order to normalise ^{14}C data to $-25‰$ $\delta^{13}C_{VPDB}$. Graphite prepared at the NERC Radiocarbon Lab was analysed by Accelerator Mass Spectrometry at the Scottish Universities Environmental Research Centre AMS (5MV NEC) (Xu et al., 2004).

4. RESULTS AND DISCUSSION

4.1. Surface and cave climate

The local meteorological station data from Mechara, Bedessa, and Gelemso are presented in Fig. 3 for the mean and standard deviation variability in mean monthly rainfall and temperature. The raw data is available in Electronic Annex EA-1. Mean monthly rainfall and temperature are similar between the three stations, demonstrating that the data are largely homogenous despite their discontinuous nature. The three stations show little seasonal variation in solar radiation, due to the low latitude of the study region and therefore little seasonal variation in surface temperature. Highest temperatures occur in late spring/early summer; between the two rainy seasons when cloud cover is relatively low. Mean annual temperature is 19.8°C at Gelemso and 19.2 °C at Bedessa. The strong seasonality in precipitation, with two rainy seasons, is typical of the region. The first rain season, centred on April, is equivalent to the regional and unreliable 'small rains'; it is highly variable with a 1 standard deviation April mean rainfall range of 60–210 mm. The second rain season occurs predominantly in July and August, and is equivalent to the reliable 'big rains' caused by the overhead passage of the ITCZ. This has a 1 standard deviation monthly mean rainfall range of 70–240 mm; again variable but with a higher mean value. Monthly mean potential evapotranspiration in the region, calculated using both Penman and Thornthwaite methods, is 65–85 mm (Wagari Furi, 2005; available as electronic annex EA-2), a value which rainfall rarely exceeds between November and February inclusive.

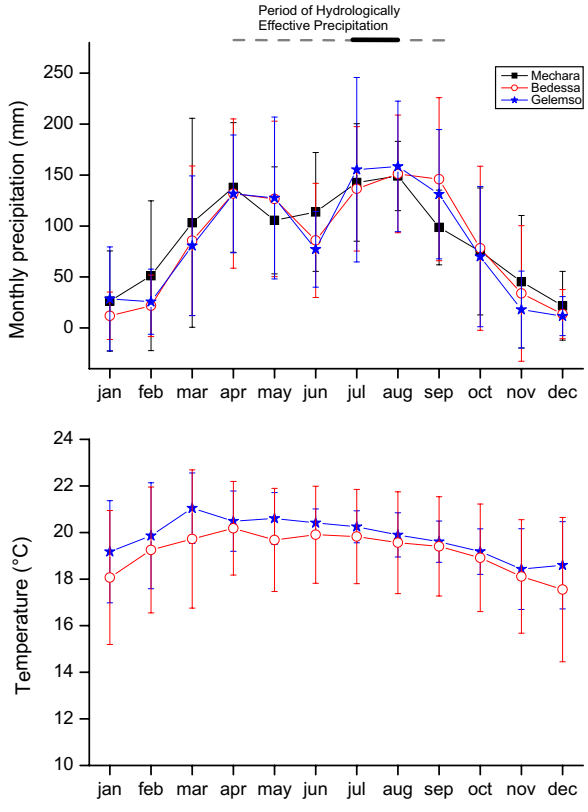

Fig. 3. Mean and standard deviation monthly rainfall and temperature series from local weather stations (locations shown in Fig. 1); data averaged for all available data (see Section 3.1).

Given the good agreement between mean monthly rainfall and the three stations, for each calendar month (January–December) we calculated an average monthly mean precipitation from all available data. We compared these values to the monthly means in the Addis Ababa series, the nearest, long, homogeneous rainfall series (homogenous since 1901; Conway et al., 2004). By applying a simple correction for each month (January: ×1.25; February: ×0.72; March: ×1.26; April: ×1.36; May: ×1.62; June: x0.73; July: ×0.57; August: ×0.52; September: ×0.67; October: ×2.13; November: ×2.92; December: ×1.15), we transformed the monthly mean precipitation values in the Addis Ababa series to that in our local rainfall series. This provides a continuous climate record for the last 100 years, against which the stalagmite climate proxies can be compared (see Section 4.3). This cross calibration demonstrates that in the Mechara region, the spring ('small') rains are greater in amount than those experienced at Addis Ababa, and summer ('big') rains relatively weak and sporadic, although they are still the most important rain period.

Cave air temperature was recorded at 30 min intervals from October 2005 to June 2006 within Asfa Chamber in Rukiessa Cave. Temperature varied from 19.2 °C in summer to 18.6 °C in winter, values matching the mean annual surface temperature. Relative humidity measured by handheld Kestral weather stations averaged $97 \pm 2\%$ ($n = 7$).

4.2. Surface and ground water geochemistry

Water isotope results are presented in Fig. 4 for surface waters, springs, and cave pool and drip waters from several caves in the region including Rukiessa Cave. Modern drip water isotope data falls on both the global and Addis Ababa meteoric water lines, and demonstrate the dominance of

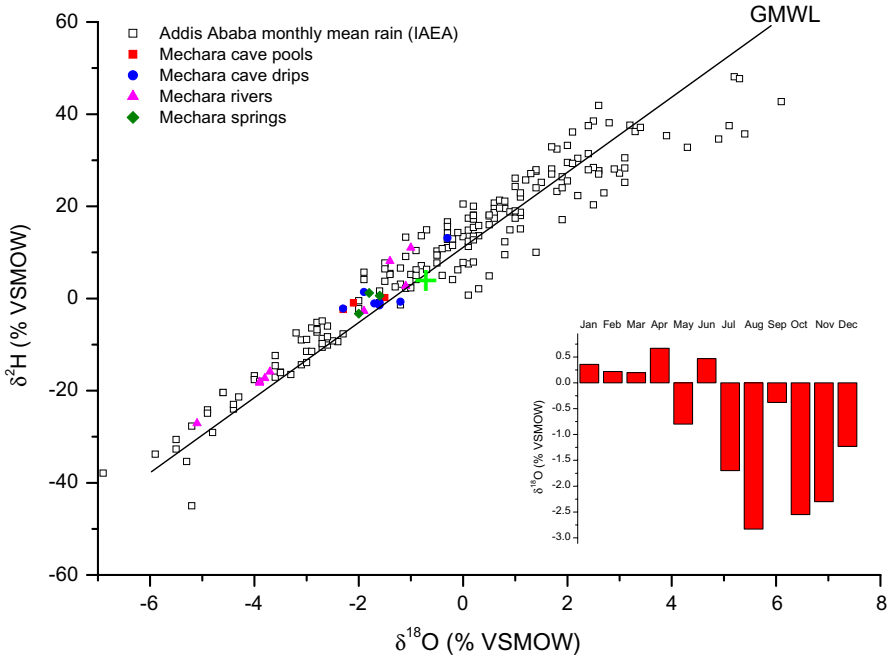

Fig. 4. $\delta^{18}O$ and δD for cave drip waters, pools, and surface rivers and springs, together with the monthly mean isotopic composition of rainfall from Addis Ababa (open squares). Monthly weighted $\delta^{18}O$ is shown in the inset, and annual weighted mean isotopic composition of rainfall is shown by the cross.

equilibrium fractionation processes rather than evaporation. Most samples cluster around the weighted annual mean value; predominantly these are cave drip waters, including those from Rukiessa Cave. Greatest isotope variability can be observed in the surface water river samples. In one case where repeat measurements of the same drip have been possible (Mercury Chamber Drip), seasonal variations of up to 2‰ in $\delta^{18}O$ are apparent, with samples collected after spring rains isotopically heavier than those collected after the summer rains, reflecting the composition of the spring rainfall and suggesting at this drip site a rapid flow component. Using observed drip water $\delta^{18}O$ and cave air temperature, and equations of O'Neill et al. (1969), Hays and Grossman (1991) and Leng and Marshall (2004) expression of Kim and O'Neil (1997) equation, then predicted equilibrium calcite $\delta^{18}O$ is −1.2‰ to −3.3‰.

Rukiessa Cave drip water geochemistry is typical of those of the region. Rukiessa Cave drip water electrical conductivity is 628 ± 261 μS cm^{-1} ($n = 11$), calcium ion concentration of 71 ± 28 ppm ($n = 6$) and magnesium ion concentration of 44 ± 29 ppm ($n = 6$); a very strong correlation is observed between electrical conductivity and calcium plus magnesium concentration. These values compare with electrical conductivity values of 950 ± 525 μS cm^{-1} ($n = 8$) at nearby Achere Cave and 555 ± 91 μS cm^{-1} ($n = 4$) in local rivers. From these values, presuming alkalinity matches calcium and magnesium ion concentration, and the observed cave temperature of ~19 °C, we can predict the modern stalagmite growth rate (Dreybrodt, 1981; Baker et al., 1998) to be in the range 0.2–0.3 mm yr^{-1} for atmospheric P_{CO_2} values (and lower growth rate if P_{CO_2} is higher).

4.3. Stalagmites

4.3.1. Texture and morphology

Fig. 2 shows the morphology and texture of the two actively growing stalagmites. Merc-1 has a broader width to height ratio than Asfa-3, suggesting that this sample experiences water flow down its sides during periods of high drip rates. Our observed drip rate data are limited to the three expeditions, but are informative. Drip rate for Merc-1 varies between 13 and 20 min per drip, demonstrating some seasonal variability. Drip rates onto Asfa-3 are much slower (the fastest drip rate observed was 1 drip every 53 min). Drip rate and morphology data suggest that it is most likely that Asfa-3 is predominantly fed by stored groundwater, whereas Merc-1 has a greater proportion of event water.

Despite differences in morphology, Asfa-3 and Merc-1 have similar appearance in hand section, with alternating growth phases dominated by light and dark coloured calcite at the centimetre-scale, as well as similar alternations at the sub millimetre scale to form regular laminae (see Section 4.3.2). The centimetre-scale colour variations correlate between samples, particularly between 22.32 and 31.58 mm (WC1 on Fig. 2) and at 5.6 mm (WC2 on Fig. 2) from top for Asfa-3 (and between 21.14 and 28.34 mm and at 5.55 mm for Merc-1), the former between 100 and 75 laminae from the top and the latter 21 laminae from the top. If the laminae are presumed annual (see Section 4.3.2), these are equivalent to 1905–1930 and around 1984 AD, periods of known famine. Colourless calcite deposition, in contrast to periods of dark calcite that are brown in colour in hand specimen, is typical of the absence of higher concentrations

of humic substances (Lauritzen et al., 1986; White and Brennan, 1989) that would be observed in wetter periods.

In thin section, the stalagmite fabric can be observed to resemble 'type 3' of Kendall and Broughton (1978) and is transitional between the columnar and microcrystalline types of Frisia et al. (2000). Both stalagmites comprise elongate columnar fabric perpendicular to growth with decimicron-scale crystallites and infrequent microscopic inclusions. The sub-millimeter scale laminae that are visible in both hand and thin section are defined by zones with multiple thin (micron-scale) laminae represented by impurities (opaque in transmitted light); where most strongly developed they drape crystallite surfaces that occasionally show some dissolution features. We hypothesize that the surfaces occur annually during the winter dry season due to drip cessation, or very slow drip rates. The groups of opaque laminae compare with infiltration laminae characterized by the input of detrital and colloidal material during periods of infiltration (Borsato et al., 2007). We thus interpret the impurity-bearing laminae as representing seasonally high flows.

4.3.2. Lamina counts

Lamina counts on each sample were performed in triplicate and the mean thickness recorded. Results are presented in Fig. 5a. A total of 94 laminae were counted in Asfa-3 from the top to a dissolutional hiatus at the base of the sample (marked on Fig. 2). One hundred and eleven laminae were counted to the base of Merc-1. Laminae typically vary between 0.2 and 0.4 mm width, with some thicker laminae in periods of colourless calcite deposition in Asfa-3. Laminae are continuous with no periods of indistinct or discontinuous laminae. This observation agrees with those expected for annual laminae for the temperature of the cave, atmospheric P_{CO_2} and calcium and magnesium concentrations of the drip waters (see Section 4.2). Also, the regularity of the laminae and the strength of the seasonal rainfall forcing would also confirm that the laminae are indeed annual. Assuming annual deposition, Asfa-3 was deposited from 1910 AD until sampled in 2004, and Merc-1 was deposited from 1894 AD until sampled in 2004 AD.

4.3.3. ^{14}C profile

Results of 6 ^{14}C analyses on each sample are presented in Table 1. Both samples clearly have rising trend in percent modern carbon towards the top. In Asfa-3, this value exceeds 100%, whereas in Merc-1 the maximum observed pMC is just over 94% (although higher values may have occurred between sample locations). This means that a contamination by bomb-^{14}C from the atmospheric nuclear tests is likely to have happened in the top layers of the samples. Because the carbon found in the speleothem has two main sources: the limestone dissolution and the soil CO_2 (produced by the organic matter degradation and by the plant root respiration), both producing HCO_3 in the seepage water, an abrupt increase in ^{14}C in recent growth laminae close to the tip of a stalagmite can be used as a control of its modernity (Genty and Massault, 1997; Genty et al., 1998, 2001). Lamina years representing 1950 AD are equivalent to ^{14}C values (pMC) of ~80% for Merc-1, and 85% for Asfa-3, indicating a 'dead carbon percentage of approximately 20% and 15%, respectively, values that are typical for cave stalagmites (Genty et al., 1998). This interpretation supports modern stalagmite deposition, agreeing with the active drip rates that contain high electrical conductivities indicative of calcite supersaturation.

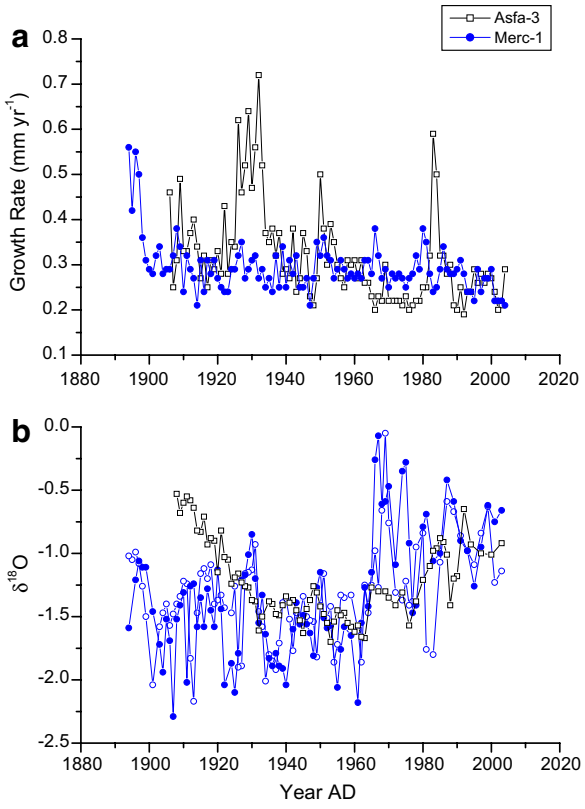

Fig. 5. Time series for growth rate (a) and $\delta^{18}O$ (b) for Asfa-3 (squares) and Merc-1 (circles). Duplicate $\delta^{18}O$ series on Merc-1 shown by open and closed circle symbols.

4.3.4. Growth rate as a climate parameter

Graphs of growth rate versus time are shown in Fig. 5a. The two stalagmites have similar mean growth rates but differing growth rate variability; Asfa-3 has a coefficient of variation of 33% and Merc-1 of 13%. In particular, Asfa-3 has a time series that shows a few years of relatively high growth rate, all are associated with phases of colourless calcite deposition, suggestive of a non-linear response to surface climate.

We compared the growth rate series of both stalagmites against the long rainfall series, initially comparing with annual, seasonal, and monthly rainfall data (the latter for March–September only, since November–February contain >15% of years where rainfall = 0). We compared growth rate with the rainfall in that calendar year, as well as against preceding years by considering both a 'classic' decadal average, as well as an appropriate linear 'climate transfer function' that reflects groundwater smoothing of a surface

Table 1
^{14}C results for stalagmites Asfa-3 and Merc-1

Publication code	Identifier	Lamina year	^{14}C enrichment (% modern $\pm 1\sigma$)	Conventional radiocarbon age (years BP $\pm 1\sigma$)
SUERC-11357	MERC-1 A	2004	94.84 ± 0.41	425 ± 35
SUERC-11359	MERC-1 B	1990	88.57 ± 0.39	975 ± 35
SUERC-11362	MERC-1 C	1980	84.16 ± 0.37	1385 ± 35
SUERC-11363	MERC-1 D	1970	82.42 ± 0.36	1553 ± 35
SUERC-11364	MERC-1 E	1960	79.75 ± 0.35	1817 ± 35
SUERC-11365	MERC-1 F	1950	79.98 ± 0.35	1795 ± 35
SUERC-7016	Asfa-3A	2004	104.39 ± 0.31	post-1950
SUERC-8070	Asfa-3	1990	103.41 ± 0.31	post-1950
SUERC-8071	Asfa-3	1980	92.61 ± 0.28	616 ± 25
SUERC-8072	Asfa-3	1970	91.13 ± 0.28	746 ± 24
SUERC-8073	Asfa-3	1960	91.50 ± 0.28	713 ± 24
SUERC-8074	Asfa-3	1950	90.23 ± 0.27	826 ± 24

climate signal. We considered that the dripwaters feeding the stalagmites comprise two components—a small proportion of fissure flow water with a rapid (same year) response to surface rainfall, and a larger proportion of stored water with a slower (decadal) response to surface rainfall (Smart and Friedrich, 1987). Proportions of event water were varied from 10% to 30%, and storage water from 70% to 90% with 5–20 years averaging of preceding rainfall. Results are summarised in Table 2, and a comparison of climate transfer functions in Fig. 7a and b.

For both samples, correlations with the current year's rainfall were weak and statistically insignificant (Table 2). Seasonal rainfall correlations were stronger, especially for Asfa-3 for which decadal averaged growth rate correlates with June–August rainfall ($r = 0.50$). Applying the climate transfer function, good correlations were observed which also exhibited a distinct pattern with the rainfall month, although there was little improvement between decadal averaging and a more complex climate transfer function, especially for Asfa-3. For Asfa-3, growth rate correlates positively with high rainfall totals in May, June, and July; and negatively with low rainfall totals in March and April. This pattern can not be explained solely by a relationship with rainfall amount, as that should lead to a positive relationship between growth rate and both of spring and summer rains. Seasonal variations in drip water or cave P_{CO_2} calcium and magnesium ion concentrations must also be important; for example in years of lower spring rainfall, limited vegetation growth, and soil CO_2 production could lead to spring rainfall derived drip waters with relatively low dissolved calcium and magnesium concentrations. In contrast to Asfa-3, only weak correlations between growth rate and climate were observed for Merc-1 (Fig. 7b). In part, this is due to the low growth rate variability observed in this sample, as well as the multitude of factors that affect growth rate, in this case cancelling out any clear climate correlation. Applying the same transfer functions as for Asfa-3, it can be seen that the function leading to the strongest correlations has a greater proportion of relatively short residence time water (20% event water, 80% stored water of <5 years). The strongest correlation is with July rainfall, again reflecting increased water availability as well as probable increased soil CO_2, but the correlation coefficient is only 0.30.

4.3.5. $\delta^{18}O$

Our modern drip water (Fig. 4) data suggest that the stalagmite samples should have $\delta^{18}O$ variations within the range $-1.2‰$ and $-3.3‰$ if they are in isotopic equilibrium, and which should primarily reflect variations in rainfall. Fig. 5b shows the $\delta^{18}O$ profiles for both stalagmites, including a replicated profile for Merc-1. Most of the data falls within the range as the predicted values for $\delta^{18}O$ calcite, although the lowest predicted values are not seen. Only when the lowest $\delta^{18}O$ calcite is precipitated from the highest $\delta^{18}O$ waters is deposition in equilibrium. Both stalagmites exhibit low frequency trends in $\delta^{18}O$. Merc-1 has a continuous increasing trend in $\delta^{18}O$, and Asfa-3 an initial decreasing

Table 2
Correlations (r values) between annual, seasonal and monthly rainfall amount and stalagmite parameters

Stalagmite	Annual P	Annual P decadal average	Spring P (March–May)	Spring P (March–May) decadal average	Summer P (June–August)	Summer P (June–August) decadal average	Monthly P decadal average
Asfa-3 growth rate	0.04	0.25	0.11	0.14	0.09	**0.50**	March (**−0.42**), April (**−0.43**) May (**0.42**), June (**0.42**) July (**0.42**)
Asfa-3 $\delta^{18}O$	0.06	0.23	0.08	0.21	−0.07	0.19	August (**0.45**)
Merc-1 growth rate	0.00	0.17	−0.05	−0.04	0.04	0.17	August (0.19)
Merc-1 $\delta^{18}O$	0.13	0.01	0.11	−0.01	−0.07	−0.20	July (**−0.32**)

Statistically significant values are shown in bold.

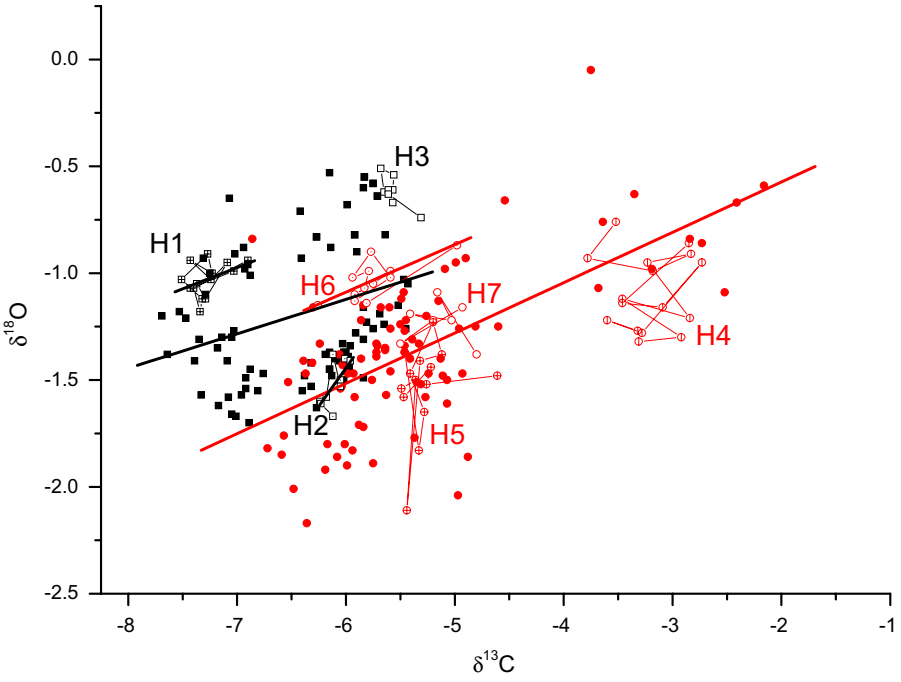

Fig. 6. Hendy test results for Merc-1 (red circles) and Asfa-3 (black squares). Filled symbols are time series data, open symbols with lines are Hendy tests along individual lamina. Where there are statistically significant relationships between $\delta^{13}C$ and $\delta^{18}O$, linear regression lines are shown. (For interpretation of the references in color in this figure legend, the reader is referred to the web version of this article.)

trend in $\delta^{18}O$ which changes in inflexion between 1940 and 1960 AD to an increasing trend in $\delta^{18}O$; differences in trend indicative of different processes affecting stored water $\delta^{18}O$ composition. Merc-1 has greater high frequency variability in $\delta^{18}O$ compared to Asfa-3, indicative of a more direct hydrological connection to the surface, and with lower proportion of storage water with respect to event water, compared to Asfa-3. Fig. 6 presents the results of $\delta^{13}C$ vs $\delta^{18}O$ analyses both along individual growth layers ('Hendy tests') as well as for both samples as a whole. Duplicate time series on Merc-1 show excellent agreement between Merc-1 profiles, and a good agreement in low frequency signal between the Asfa-3 and Merc-1 time series. The low variability in Asfa-3 reflects storage effects as demonstrated by the low drip rates and the fact that the best climate transfer function between growth rate and surface climate had the greatest proportion of stored water (90% was an average of the preceding 10 years, with no statistical difference between this transfer function and a simple decadal averaging). In contrast, there is significant annual to multi-annual variability in the Merc-1 $\delta^{18}O$ (despite constant growth rate), indicative of a greater proportion of event water.

Fig. 6 demonstrates that for both Asfa-3 and Merc-1, there is a general positive correlation between $\delta^{13}C$ and $\delta^{18}O$, a result generally indicative of possible non-equilibrium deposition. The results of the Hendy tests also show a positive correlation between $\delta^{18}O$ and $\delta^{13}C$ for some lamina, with variations of both $\delta^{18}O$ and $\delta^{13}C$ within an individual lamina (shown by open symbols with line) of up to 1‰. Two out of three Hendy tests on Asfa-3 have a positive correlation, and these are situated within dark coloured calcite, for which it has been hypothesised that disequilibrium effects would be less likely. For Merc-1, a positive correlation between $\delta^{13}C$ and $\delta^{18}O$ is only observed in one lamina out of the four tested, and that is situated in white calcite. Hendy tests therefore suggest that Asfa-3 might be expected to exhibit non-equilibrium behaviour for the whole of its deposition period. Merc-1 will also be expected to exhibit non-equilibrium behaviour, although possibly more within periods of colourless calcite deposition. There are two processes that are likely to cause disequilibrium; these are high supersaturation, leading to rapid degassing such that the oxygen isotope composition of the speleothem carbonate ($\delta^{18}O_c$) is out of equilibrium with the oxygen isotope composition of the drip water ($\delta^{18}O_w$), or evaporation on the stalagmite cap during degassing (Mickler et al., 2004). Both processes are possible. Both modern day drip water dissolved calcium concentration and stalagmite growth rates are high, suggesting that disequilibrium during degassing is possible. Evaporative effects are also possible, although our survey of modern day cave climate in Rukiessa shows that relative humidity is >90%. Additionally, we note that $\delta^{18}O$ is less variable than $\delta^{13}C$ in this sample. Typically, with all other factors held constant, kinetic fractionation leads to a greater variability of $\delta^{13}C$ than $\delta^{18}O$. An exception is during evaporation, where $H_2{}^{16}O$ is preferentially lost by this process, in addition to any degassing disequilibria in the H_2O–CO_2 system.

We investigated the correlations between annual, seasonal and monthly rainfall and $\delta^{18}O$ in both Asfa-3 and Merc-1, and applied climate transfer functions as in Section 4.3.4. Results are presented in Table 2 and Fig. 7. Both stalagmites exhibit statistically significant correlations with monthly rainfall, especially when decadal averaging or the

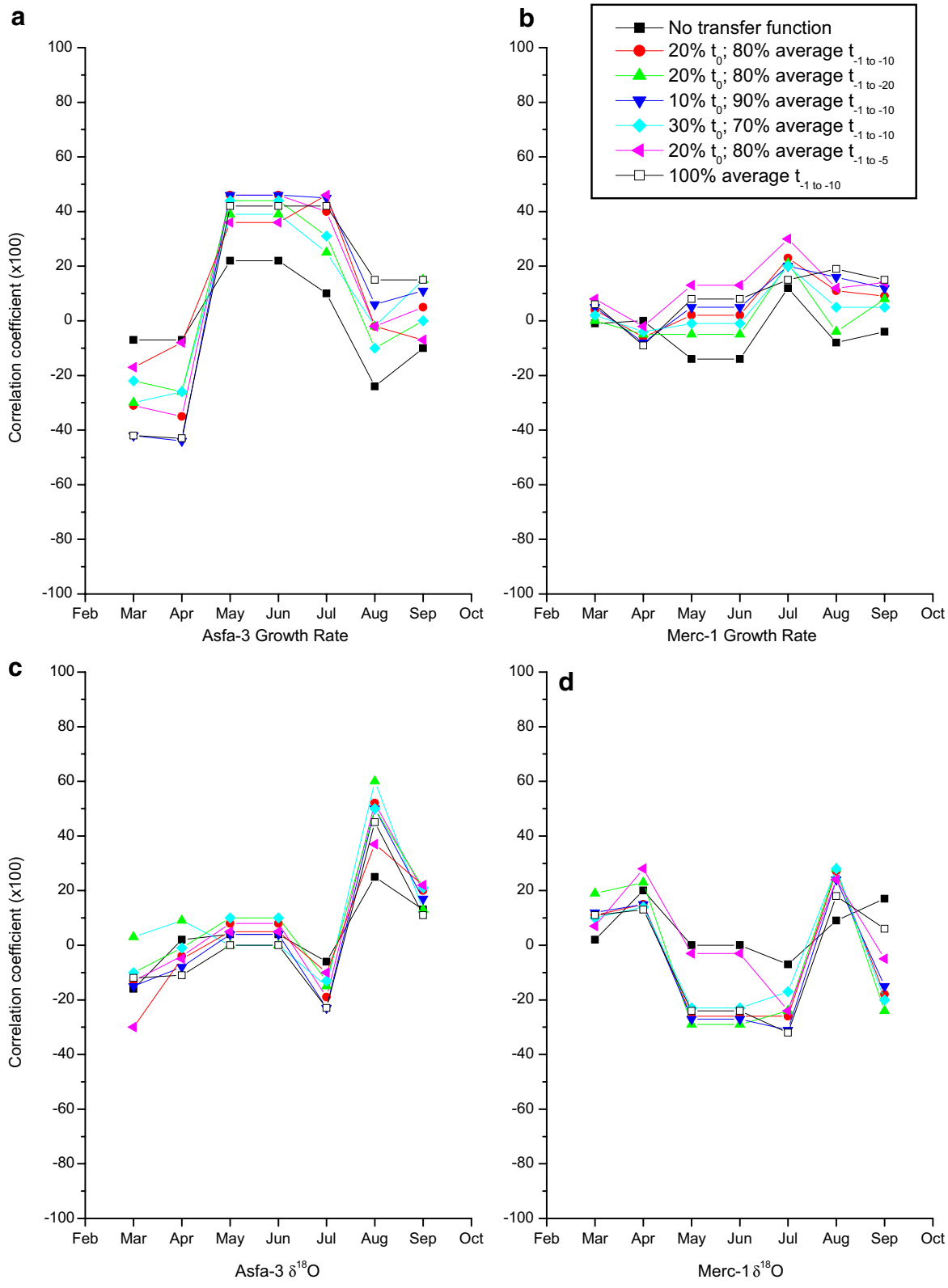

Fig. 7. Correlation coefficients between monthly rainfall and stalagmite parameters. (a) Asfa-3 growth rate (b) Merc-1 growth rate (c) Asfa-3 $\delta^{18}O$ and (d) Merc-1 $\delta^{18}O$.

climate transfer functions have been applied. When compared with the instrumental rainfall series, Asfa-3 exhibited a strong positive correlation with August rainfall, with correlation coefficients of 0.55 with the same climate transfer function as for growth rate. High rainfall totals in August, at the end of the second rain season (the 'big rains') would maintain drip waters into the following dry season. Although relatively isotopically light, these waters might be more prone to evaporation or kinetic fractionation effects. In contrast, Merc-1 exhibits a weak but significant negative correlation with July rainfall and $\delta^{18}O$ (Fig. 7d) and weak but significant positive correlation with April and August $\delta^{18}O$. These relationships are in part the same as for Asfa-3; positive correlations with the spring rains are due to a greater amount of this isotopically heavy water reaching the stalagmite, and the positive correlation with August rainfall is again hypothesised to be a disequilibrium effect. The negative correlation with rainfall amount in the summer rain season is due to a greater proportion of isotopically light rainfall reaching the stalagmite. Correlations for individual months are relatively weak at ~0.3; however the ratio of spring (April) to summer (July) rains and the same climate transfer function as for growth rate (20% event water, 80% waters of <5 years) yields a stronger correlation of 0.49, and a better correlation than using decadal averaging.

We apply the correlations, with error uncertainties based on the correlation coefficients (from Sections 4.3.4 and 4.3.5), and in transforming the rainfall series (from Section 4.1), to hindcast monthly or seasonal rainfall totals, as shown in Fig. 8. Fig. 8a presents long-term changes in the balance of spring to summer rains, reconstructed from Merc-1 $\delta^{18}O$ and applying a transfer function of 20% event water, 80% waters of <5 years, and showing a gradual increase in relative amount of spring (April) rainfall, as reflected in the low frequency trend to more positive $\delta^{18}O$ in this stalagmite (Fig. 5b). Fig. 8b shows reconstructed May–July rainfall from Asfa-3 growth rate variations, applying a transfer function of 10% event water, 90% waters of <10 years. This shows the gradual decline in summer rainfall that has in part led to increased drought and famine in East Africa; the available instrumental records that show a general decline in rainfall amount in eastern Ethiopia, especially since the 1980s (Seleshi and Zanke, 2004) and soil studies in Northern Ethiopia also shows a general increase in drought frequency and aridity over the last 1000 years, especially since the 17th century (Machado et al., 1998). The growth rate hindcast performs worst in

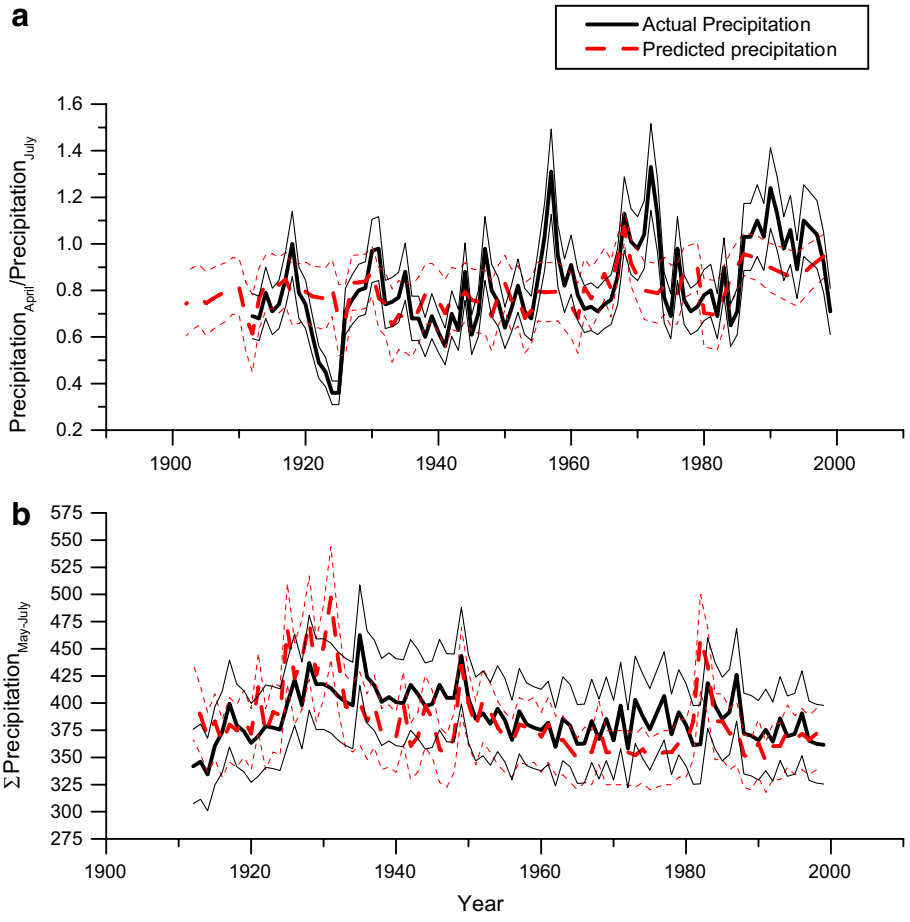

Fig. 8. Reconstructed precipitation records from stalagmites Asfa-3 and Merc-1. (a) Ratio of April–July rainfall reconstructed from Merc-1 ^{18}O. (b) May–July rainfall reconstructed from Asfa-3 growth rate. Errors on actual precipitation are based on a 10% transfer function error.

periods of highest growth rate, where rainfall amounts are slightly over-predicted. This suggest that there may be a non-linearity in the summer rainfall—growth rate correlation, where years of growth rate >0.5 mm yr^{-1} are not explained by the instrumental climate calibration, and that for this sample only periods of slower growth rate should be used to reconstruct past rainfall.

5. CONCLUSIONS

There is currently an intense focus on the last 1000 years, as a representative of background climate behaviour against which to judge current changes. Key debates revolve around the rate of change of temperature changes in the past, as this has implications for the relative importance of natural and anthropogenic forcing. Although considering rainfall rather than temperature, we show that multiple parameters from individual stalagmite have different climate sensitivities and would yield contrasting proxy—climate forcing functions. Multi-parameter, multi-proxy approaches are essential when using stalagmites to reconstruct climate due to the individual nature of the link between surface climate and cave stalagmite due to the heterogeneity and complexity of karst groundwater flow (Fairchild et al., 2006a; Baker and Brunsdon, 2003). Some stalagmites respond more to high frequency ('event') climate (in our case, Merc-1), others low frequency ('storage') climate (in our case Asfa-3), due to differences in their relative contributions to the stalagmite drip waters. Different parameters also respond to different seasons, and in some cases the same parameter responds to different months or seasons via different forcing mechanisms (e.g., rainfall seasonality or amount, or non-equilibrium factors). Coarsening of the $\delta^{18}O$ series presented in Fig. 5 to mimic lower resolution stalagmite climate reconstructions would still preserve these differences between stalagmite $\delta^{18}O$. Therefore, variations in $\delta^{18}O$ between stalagmites with supra annual sampling resolution, due to cooler temperatures and slower growth rate, but in regions that have similar rainfall seasonality, could also be explained by the processes observed here. In general, for our stalagmites, comparison with monthly or seasonal mean rainfall yields the highest correlations with the parameters ^{18}O and growth rate. With water availability rather than temperature the crucial issue in semi-arid areas such as lowland parts of Ethiopia, we propose that multi-parameter, multi-proxy analyses of long time series from speleothems offer a most promising approach to characterizing the variability of rainfall in this densely populated region, which furthermore offers important scientific challenges in the understanding the dynamics of rainfall variability.

ACKNOWLEDGMENTS

Research was supported by a Philip Leverhulme Prize to A.B., a Royal Society International Exchange Grant to A.A. and A.B., NERC Grants (Radiocarbon 1096.1004; Standard NE/C511805/1; ICP 055299) to A.B. and I.J.F., and a START Grant to A.A. We thank Hailu Dibabe and Jo Baker for field support, Hilary Sloane for the isotope analyses, Paul Hands for thin sectioning, Henry Lamb for Fig. 1, and Ming Tan and two anonymous referees for comments on the manuscript.

APPENDIX A. SUPPLEMENTARY DATA

Supplementary data associated with this article can be found, in the online version, at doi:10.1016/j.gca.2007.03.029.

REFERENCES

Asrat A. (2002) The rock-hewn churches of Central and Eastern Tigrai: a geological perspective. *Geoarchaeology* **17**, 649–663.

Asrat A., Baker A., Umer M., Leng M. J., van Calsteren P., and Smith C. (2007) A high-resolution multi-proxy stalagmite record from Mechara, Southeastern Ethiopia: palaeohydrological implications for speleothem palaeoclimate reconstruction. *J. Quatern. Sci.* **22**(1), 53–63.

Baker A., and Brunsdon C. (2003) Non-linearities in drip water hydrology: an example from stump cross caverns, Yorkshire. *J. Hydrol.* **277**, 151–163.

Baker A., Genty D., Dreybrodt W., Grapes J., and Mockler N. J. (1998) Testing theoretically predicted stalagmite growth rate with recent annually laminated stalagmites: implications for past stalagmite deposition. *Geochim. Cosmochim. Acta* **62**, 393–404.

Borsato A., Frisia S., Fairchild I. J., Somogyi A., and Susini J. (2007) Trace element distribution in annual stalagmite laminae mapped by micrometer-resolution X-ray fluorescence: implications for incorporation of environmentally significant species. *Geochim. Cosmochim. Acta* **71**(6), 1494–1512.

Bosellini A., Russo A., Fantozzi P. L., Assefa G., and Tadesse S. (1997) The Mesozoic succession of the Mekele Outlier (Tigrai Province, Ethiopia). *Mem. Sci. Geolog.* **49**, 95–116.

Brown, L., Gunn, J., Walker, C., Williams, O. (1998) *Cave Ethiopia '95 and '96 Expedition Report*. University of Huddersfield, UK. 28pp.

Burns S. J., Fleitmann D., Mudelsee M., Neff U., Mangini A., and Matter A. (2002) A 780-year annually resolved record of Indian Ocean monsoon precipitation from a speleothem from south Oman. *J. Geophys. Res.* **107**(D20), 4434.

Camberlin P., and Philippon N. (2002) The East African March–May rainy season, its teleconnections and predictability over the 1968–1997 period. *J. Clim.* **15**, 1002–1019.

Conway D., Mould C., and Bewket W. (2004) A century of climate observations at Addis Ababa, Ethiopia. *Int. J. Climatol.* **24**, 77–91.

Dreybrodt W. (1981) The kinetics of calcite deposition from thin films of natural calcareous solutions and the growth of speleothems: revisited. *Chem. Geol.* **32**, 237–245.

Dreybrodt W. (1988) *Processes in karst systems*. Wiley, NEWYork, 288.

Dreybrodt W., and Franke H. W. (1987) Wachstumsgfeschwindigkeit und Durchmesser von Kerzenstalagmiten. *Die Höhle* **38**, 1–6.

Fairchild I. J., Smith C. L., Baker A., Fuller L., Spötl C., Mattey D., McDermott F., and E.I.M.F. (2006a) Modification and preservation of environmental signals in speleothems. *Earth Science Reviews* **75**, 105–153.

Fairchild I. J., Tuckwell G. W., Baker A., and Tooth A. F. (2006b) Modelling of dripwater hydrology and hydrogeochemistry in a weakly karstified aquifer (Bath, UK): implications for climate change studies. *J. Hydrol.* **321**, 213–231.

Fleitmann D., Burns S. J., and Mudelsee M. (2003) Holocene forcing of the Indian monsoon recorded in a stalagmite from Southern Oman. *Science* **300**, 1737–1739.

Frisia S., Borsato A., Fairchild I. J., and McDermott F. (2000) Calcite fabrics, growth mechanisms, and environments of formation in speleothems from the Italian Alps and Southwestern Ireland. *J. Sediment. Res.* **70**, 1183–1186.

Frisia S., Borsato A., Fairchild I. J., McDermott F., and Selmo E. M. (2002) Aragonite-calcite relationships in speleothems (Grotte de Clamouse, France): environment, fabrics, and carbonate geochemistry. *J. Sediment. Res.* **72**(5), 687–699.

Gams I. (1981) Contribution to the morphometrics of stalagmites. *Proc. 8th Int. Congr. Speleol.*, 276–278.

Genty D., and Massault M. (1997) Bomb ^{14}C recorded in laminated speleothems—part 1: dead carbon proportion calculation. *Radiocarbon* **39**, 33–48.

Genty D., and Massault M. (1999) Carbon transfer dynamics from bomb-^{14}C and d^{13}C time series of a laminated stalagmite from SW France—modelling and comparison with other stalagmite records. *Geochim. Cosmochim. Acta* **63**, 1537–1548.

Genty D., and Quinif Y. (1996) Annually laminated sequences in the internal structure of some Belgian stalagmites—importance for paleoclimatology. *J. Sediment. Res.* **66**, 275–288.

Genty D., Baker A., and Barnes W. L. (1997) Comparaison entre les lamines luminescentes et les lamines visibles annuelles de stalagmites. *Comptes Rendus Acad. Sci. II* **325**, 193–200.

Genty D., Vokal B., Obelic B., and Massault M. (1998) Bomb ^{14}C time history recorded in two modern stalagmites—importance for soil organic matter dynamics and bomb ^{14}C distribution over continents. *Earth Planet. Sci. Lett.* **160**, 795–809.

Genty D., Baker A., and Vokal B. (2001) Inter and intra annual growth rates of European stalagmites. *Chem. Geol.* **176**, 193–214.

Gillespie R., Streetperrott F. A., and Switsur R. (1983) Post-glacial arid episodes in Ethiopia have implications for climate prediction. *Nature* **306**, 680–683.

Glantz M. H. (1996) *Currents of change: El Niño's impact on climate and society*. Cambridge University Press, Cambridge UK.

Hays P. D., and Grossman E. L. (1991) Oxygen isotopes in meteoric calcite cements as indicators of continental paleoclimate. *Geology* **19**, 441–444.

Kaufmann G., and Dreybrodt W. (2004) Stalagmite growth and paleoclimate: an inverse approach. *Earth Planet. Sci. Lett.* **224**, 529–545.

Kendall A. C., and Broughton P. L. (1978) Origin of fabrics in speleothems composed of columnar calcite crystals. *J. Sediment. Petrol.* **48**, 519–538.

Kim S. T., and O'Neil J. R. (1997) Equilibrium and nonequilibrium oxygen isotope effects in synthetic carbonates. *Geochim. Cosmochim. Acta* **61**(16), 3461–3475.

Lamb H. F. (2001) Holocene climatic change and vegetation response inferred from the sediments of Ethiopian crater lakes. *Proc. R. Irish Acad.* **101B**, 35–46.

Lamb A. L., Leng M. J., Lamb H. F., Telford R. J., and Mohammed U. M. (2002) Climatic and non-climatic effects on the $\delta^{18}O$ and $\delta^{13}C$ composition of Lake Awassa, Ethiopia, during the last 6.5 Ka. *Quaternary Sci. Rev.* **21**, 2199–2211.

Lauritzen S. E., Ford D. C., and Schwarz H. P. (1986) Humic substances in a speleothem matrix. *Proc. 9th Int. Congr. Speleol.*, 77–79.

Leng M. J., and Marshall J. D. (2004) Palaeoclimate interpretation of stable isotope data from lake sediment archives. *Quaternary Sci. Rev.* **23**, 811–831.

Leng M. J., Heaton T. H. E., Lamb H. F., and Naggs F. (1998) Carbon and Oxygen isotope variability within the shell of an African land snail (Limicolaria kambeul chudeaui Germain): a high-resolution record of rainfall seasonality? *The Holocene* **8**, 407–412.

Machado M. J., Perez-Gonzalez A., and Benito G. (1998) Paleoenvironmental changes during the last 4000 yr in the Tigray. *Northern Ethiopia. Quaternary Res.* **49**, 312–321.

McDermott, F., Schwarcz, H. P., and Rowe, P. J. (2005) Isotopes in speleothems. In *Isotopes in Palaeoenvironmental Research, vol. 10*. (ed. M. Leng). Springer, Dordrecht, The Netherlands, pp. 185–226.

Mickler P. J., Banner J. L., Stern L., Asmeroml Y., Edwards R. L., and Ito E. (2004) Stable isotope variations in modern tropical speleothems: evaluating equilibrium vs. kinetic isotope effects. *Geochim. Cosmochim. Acta* **68**(21), 4381–4393.

Mohammed, M. U., Legesse, D., Gasse, F., Bonnefille, R., Lamb, H. F., Leng, M., and Lamb, A. L. (2004) In *Past climate variability through Europe and Africa* (ed. R.W. Battarbee). Springer-Verlag, Dordrecht, the Netherlands. pp. 159–180.

Neff U., Burns S. J., Mangini A., Mudelsee M., Fleitmann D., and Matter A. (2001) Strong coherence between solar variability and the monsoon in Oman between 9 and 6 kyr ago. *Nature* **411**, 290–293.

Nicholson S. E. (2000) The nature of rainfall variability over Africa on time scales of decades to millennia. *Global Planet. Change* **26**, 137–158.

O'Neill J. R., Clayton R. N., and Mayeda T. K. (1969) Oxygen isotope fractionation in divalent metal carbonates. *J. Chem. Phys.* **51**, 5547–5558.

Raisback L. B., Brook G. A., Chen J., Kalin R., and Fleisher C. J. (1994) Environmental control on the petrology of a late Holocene speleothem from Botswana with annual layer of aragonite and calcite. *J. Sediment. Res.* **64**, 147–155.

Seleshi Y., and Zanke U. (2004) Recent changes in rainfall and rainy days in Ethiopia. *Int. J. Climatol.* **24**, 973–983.

Slota P. J., Jull A. J. T., Linick T. W., and Toolin L. J. (1987) Preparation of small samples for ^{14}C accelerator targets by catalytic reduction of CO. *Radiocarbon* **29**, 303–306.

Smart, P. L., and Friedrich, H., (1987). Water movement and storage in the unsaturated zone of a maturely karstified aquifer, Mendip Hills, England. In *Proceedings of Conference in Environmental Problems in Karst Terrains and their Solution*, Bowling Green, Kentucky, pp. 57–87.

Tan M., Baker A., Genty D., Smith C., Esper J., and Cai B. (2006) Applications of stalagmite laminae to paleoclimate reconstructions: comparison with dendrochronology/climatology. *Quat. Sci. Rev.* **25**, 2103–2117.

Wagari Furi (2005). Groundwater productivity and the hydrology of dry lakes basin in North-Central sector of East Harrarghe Zone. Unpubl. MSc. Thesis, Addis Ababa University, 89pp.

Wang Y., Cheng H., Edwards R. L., He Y., Kong A., An Z., Wu J., Kelly M. J., Dykoski C. A., and Li X. (2005) The holocene Asian monsoon: links to solar changes and North Atlantic climate. *Science* **308**, 854–857.

White W. B., and Brennan E. S. (1989) Luminescence of speleothems due to fulvic acid and other activators. *Proceedings of the 10th International Congress of Speleology*, 212–214.

Xu S., Anderson R., Bryant C., Cook G. T., Dougans A., Freeman S., Naysmith P., Schnabel C., and Scott E. M. (2004) Capabilities of the New SUERC 5MV AMS Facility for ^{14}C dating. *Radiocarbon* **46**, 59–64.

Associate editor: Miryam Bar-Matthews